ISSN 0023-1584, Kinetics and Catalysis, 2009, Vol. 50, No. 2, pp. 192–198. © Pleiades Publishing, Ltd., 2009.
Original Russian Text © O.A. Bulavchenko, S.V. Cherepanova, V.V. Malakhov, L.S. Dovlitova, A.V. Ishchenko, S.V. Tsybulya, 2009, published in Kinetika i Kataliz, 2009, Vol. 50, No. 2, pp. 205–211.

In Situ XRD Study of Nanocrystalline Cobalt Oxide Reduction

O. A. Bulavchenko[a], S. V. Cherepanova[a], V. V. Malakhov[a, b], L. S. Dovlitova[a], A. V. Ishchenko[a], and S. V. Tsybulya[a, b]

[a] *Boreskov Institute of Catalysis, Siberian Branch, Russian Academy of Sciences, Novosibirsk, 630090 Russia*
[b] *Novosibirsk State University, Novosibirsk, 630090 Russia*
e-mail: isizy@catalysis.ru

Received November 20, 2007

Abstract—The reduction of nanocrystalline cobalt oxide samples (single-phase and supported on γ-Al_2O_3) was studied using in situ X-ray diffraction (XRD) analysis. The atomic structures of single-phase and supported Co_3O_4 samples were refined, and the occurrence of cationic vacancies was demonstrated. A set of methods (XRD, temperature-programmed reduction, and differential dissolution) was used to find that the reduction of supported and unsupported model cobalt oxide was considerably different. The single-phase sample was reduced in undiluted hydrogen to cobalt metal with a hexagonal closely packed structure. The reduction of the supported sample (unlike the single-phase sample) occurred through the formation of a crystalline CoO phase to the formation of cobalt metal with a face-centered cubic structure. Interaction of cobalt oxide with the γ-Al_2O_3 support, which hinders the reduction to cobalt metal, was detected.

DOI: 10.1134/S0023158409020086

INTRODUCTION

The synthesis of hydrocarbons from CO and H_2 is a process for the production of artificial liquid fuel and valuable chemicals from nonpetroleum raw materials (coal, natural gas, and biomass). This synthesis is well known as Fischer–Tropsch synthesis, which occurs with the participation of catalysts containing Group VIII transition metals. The most promising catalysts are cobalt-containing systems, which are selective toward the formation of linear alkanes [1].

Co_3O_4, which is activated by hydrogen, is the catalyst precursor. The reduction of Co_3O_4 is of interest for determining the regularities of the formation of the active state of the catalyst and for regulating the degree of dispersion and structure depending on process conditions.

The reduction of cobalt oxide supported on various materials has been considered in detail in the literature. Temperature-programmed reduction (TPR) has mainly been used for these studies [2–8]. As a rule, TPR profiles contained two peaks for various supports (γ-Al_2O_3, SiO_2, and TiO_2). The ratio between the areas of the first and second peaks was close to 1 : 3, which is consistent with the stoichiometry of Co_3O_4 reduction in two steps: the first step is the reduction of Co_3O_4 to CoO, and the second step is the reduction of CoO to Co. The low-temperature peak was usually narrow; this fact suggests rapid conversion into CoO. The high-temperature peak was broad; this fact suggests a hindered reduction of CoO to cobalt metal. Previously [7, 9], this was explained by the fact that the kinetics of CoO reduction strongly depends on the initial particle size of Co_3O_4 because the rate of reduction of smaller particles was much lower because of their interaction with the support. The above interaction led to the fact that a portion of the cobalt oxide was difficult to reduce completely.

The reduction of nanocrystalline single-phase Co_3O_4 samples has received little attention in the literature. Most TPR data have been compared with those for supported catalysts. It is believed that the reduction of single-phase cobalt oxide samples occurs in two steps, as is the case with supported catalysts [10].

From the structural standpoint, the mechanisms of reduction of both supported and bulk samples have not been adequately investigated. To understand the dependence of the structure, particle size, and ratio between the resulting phases on catalyst treatment conditions (atmosphere, temperature, reduction time, and heating mode) and to control these characteristics, which affect the activity, selectivity, and stability of the catalyst, the mechanism of reduction should be explored on macro and micro levels; that is, structural changes that occur at various steps of reduction should be determined. For this purpose, structural changes should be monitored in supported catalysts and a model bulk cobalt oxide in the course of reduction. However, the ex situ studies of these systems are inadequate because nanosized cobalt particles are reoxidized in air.

The aim of this work was to study in situ the main steps of reduction of nanocrystalline cobalt oxide in single-phase (model samples) and supported states and factors affecting the process of reduction.

Table 1. Preparation procedures and the microstructure of the initial samples

Sample	Preparation procedure	S_{sp}, m^2/g	CSR, Å
Co_3O_4(1)	Prepared from $Co(OH)_2CO_3$ by decomposition in air at T = 300°C	100	140
Co_3O_4(2)	Prepared from sample (1) by calcination in air at T = 500°C for 4 h	22.3	310
Co_3O_4(3)	analytical grade (commercial reagent)	22.5	330
Co_3O_4(4)	analytical grade (commercial reagent)	16.0	320
Co_3O_4/γ-Al_2O_3(5)	Prepared from $Co(NO_3)_2$ by impregnation followed by thermal decomposition at T = 250°C. The sample contained 18% Co	–	130

EXPERIMENTAL

Sample preparation. Co_3O_4 samples were prepared in various ways. Table 1 summarizes the preparation procedures.

BET method. Data on the pore structures were obtained at a low temperature (77 K) using N_2 adsorption on a DigiSorb-2600 instrument (Micromeritics, United States). The sample was prepurified by heating at 200°C for 5 h. The experimental isotherms were treated by the BET method, which allowed us to calculate specific surface areas.

Temperature-programmed reduction. TPR was performed in a flow system with a thermal conductivity detector. Before the reduction, the samples (fraction of 0.25–0.50 mm) were trained in a flow of oxygen at 500°C for 0.5 h and cooled to room temperature in oxygen. The samples were heated at rates of 10 and 2 K/min to 900°C; the flow rate of the reducing mixture (10% H_2 in argon) was 40 cm^3/min.

Electron microscopy. High-resolution bright- and dark-field electron microscopy was used to obtain detailed information on the morphology and microstructure of catalyst samples. A JEM 2010 transmission electron microscope with a line resolution of 0.14 nm and an accelerating voltage of 200 kV was used for these studies. The identification and structural characterization of phases were performed with the use of selected-area electron diffraction. Numerical Fourier analysis was used to analyze high-resolution electron micrographs.

Differential dissolution. The phase composition was determined by differential dissolution in a flow stoichiographic system under conditions of stoichiographic titration [11, 12]. The sample weight was 10 mg. The dynamic mode of the dissolution of the initial samples consisted of changing the solvent composition from HCl with pH 2 to 1.2 M HCl and then to 3.0 M HCl and a solution of an H_2O–HCl–H_2SO_4 acid mixture (1 : 1 : 1). In the dissolution of the reduced samples, the solvent composition was varied from HCl with pH 2 to 1.2 M HCl and then to HNO_3 (HNO_3/H_2O = 1 : 1) and HF (HF/H_2O = 1 : 5). The dissolution was performed at a constant temperature of 85°C; the solvent flow rate was 2 ml/min; the time taken for the complete dissolution of a weighed sample was about 90 min.

X-ray diffraction. The in situ XRD studies were performed under conditions of reduction with hydrogen on a Siemens D500 diffractometer (CuK_α radiation) equipped with a high-temperature reactor chamber, which was developed at the Boreskov Institute of Catalysis, Siberian Branch, Russian Academy of Sciences [13]. The heating rate was 25 K/min; the hydrogen pressure was 1 atm; and the hydrogen flow rate was 600 cm^3/min. The gas mixture composition was as follows: pure hydrogen or hydrogen diluted with helium (6% H_2 + 94% He).

XRD patterns were obtained by point scanning over the angle range 2θ = 15°–70° with 2θ = 0.05° increments and an accumulation time of 5 s at each point.

To determine the minimum temperature of reduction in a flow of hydrogen, the measurements were performed repeatedly over the angle range 2θ = 30°–50° (the most intense reflections from the Co_3O_4, CoO, hcp Co, and fcc Co phases occur in this range). If reflections from CoO and/or Co did not appear at a given temperature, the temperature was increased by 10 K. The reaction temperature was increased until the appearance of reflections from a new phase. The onset of reduction was detected by the appearance of reflections from corresponding crystalline phases. The sizes of coherent scattering regions (CSRs) were calculated from the integrated widths of diffraction lines using the Selyakov–Scherrer formula.

RESULTS AND DISCUSSION

Initial Cobalt Oxide Samples

XRD analysis. Figure 1 shows the XRD patterns of the samples. The diffraction patterns of samples 1–4 correspond to a Co_3O_4 phase with various CSR sizes (Fig. 1, curves *4–7*). The overlapping of diffraction peaks due to Co_3O_4 and γ-Al_2O_3 was observed in a supported sample (Fig. 1, curve *2*); therefore, we constructed a difference curve (curve *3*) by subtracting the contribution of aluminum oxide (curve *1*) from the XRD pattern of the supported catalyst (curve *2*); this difference curve corresponds to the diffraction pattern of Co_3O_4. Normalization was performed using the most intense reflection of γ-Al_2O_3 (440).

Microstructure analysis. Table 1 summarizes the specific surface areas and average CSR sizes obtained

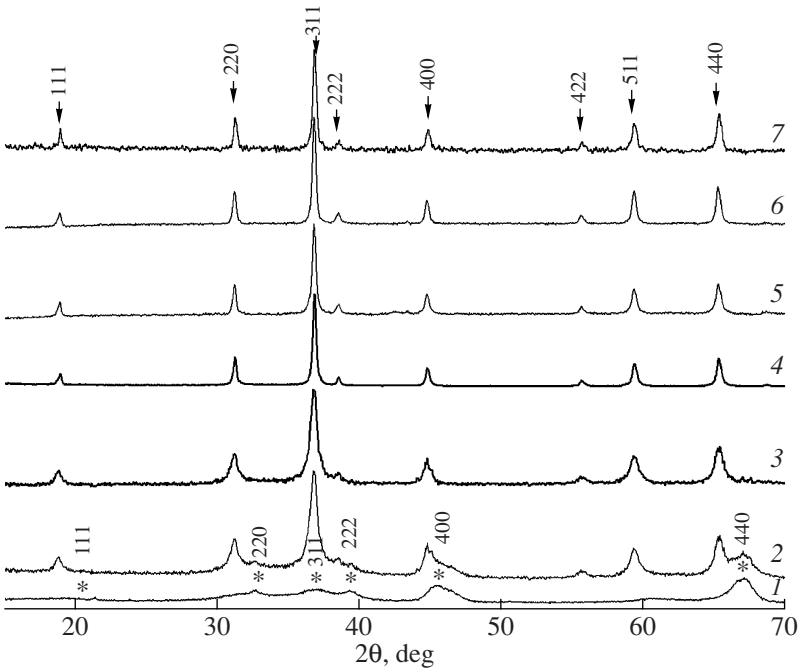

Fig. 1. XRD patterns of (*1*) γ-Al_2O_3; (*2*) Co_3O_4/γ-Al_2O_3(5); (*3*) the result of subtracting *1* from *2*; (*4*) Co_3O_4(1); (*5*) Co_3O_4(2); (*6*) Co_3O_4(3); and (*7*) Co_3O_4(4). Sample numbers in Table 1 are specified in parentheses. Arrows and asterisks indicate reflections from the Co_3O_4 and γ-Al_2O_3 phases, respectively.

from diffraction data for the test samples. The average CSR sizes were calculated from the halfwidth of the reflection (220). The sizes of the crystalline blocks (CSRs) of single-phase samples correlated well with the specific surface areas and occurred in the nanometer region (<40 nm); that is, the single-phase samples were aggregates of nanosized particles. One of the single-phase samples of Co_3O_4, namely, Co_3O_4(1), and the supported sample Co_3O_4/γ-Al_2O_3(5) had approximately the same average CSR size (Table 1).

XRD. The Co_3O_4 oxide had a spinel structure (space group *Fd*3*m*; crystallochemical formula $Co^{2+}Co_2^{3+}O_4$), where Co^{2+} occurs in the tetrahedral position 8a (1/8, 1/8, 1/8), and Co^{3+} occurs in the octahedral position 16d (1/2, 1/2, 1/2).

Table 2 summarizes the results of refining the structure of the initial samples. These data indicate that a large number of vacancies in both tetrahedral and octahedral positions (the occupancy of positions was much lower than 1) were detected in all of the test samples of cobalt oxide regardless of their different origins. Moreover, the samples Co_3O_4(2) and Co_3O_4(3) exhibited cobalt atoms occurring in an additional (nonspinel) octahedral position 16c (0,0,0).

The XRD data indicate that the electric neutrality condition is formally unsatisfied in the test cobalt oxide samples because of a deficiency of cations. Hypothetically, an excessive negative charge is compensated by the partial transition of Co^{2+} to Co^{3+} and the presence of residual carbonate and nitrate groups in the samples.

Sample Reduction

In situ XRD in a flow of 100% H_2. The in situ XRD studies were performed at various steps of the process in order to determine the minimum reduction temperature and the crystal structure. Reduction was performed in an atmosphere of hydrogen. The minimum reduction

Table 2. Occupancy parameters of the initial samples

Sample	Position	Position occupancy	Co/O (according to XRD data)
Co_3O_4(1)	8a	0.77	0.60
	16d	0.81	
	16c	0–0.01	
Co_3O_4(2)	8a	0.77	0.62
	16d	0.82	
	16c	0.05	
Co_3O_4(3)	8a	0.81	0.64
	16d	0.85	
	16c	0.04	
Co_3O_4(4)	8a	0.87	0.64
	16d	0.84	
	16c	0–0.01	
Co_3O_4/γ-Al_2O_3(5)	8a	0.80	0.57
	16d	0.72	
	16c	0–0.01	

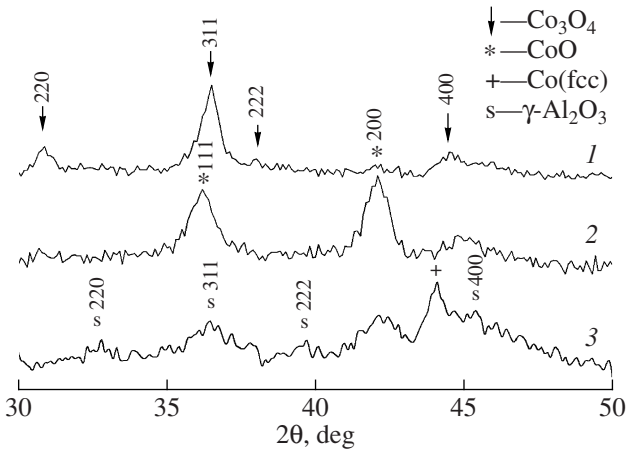

Fig. 2. XRD patterns of sample 5 (Co_3O_4/γ-Al_2O_3) in the course of reduction at (*1*) 25, (*2*) 190, and (*3*) 350°C.

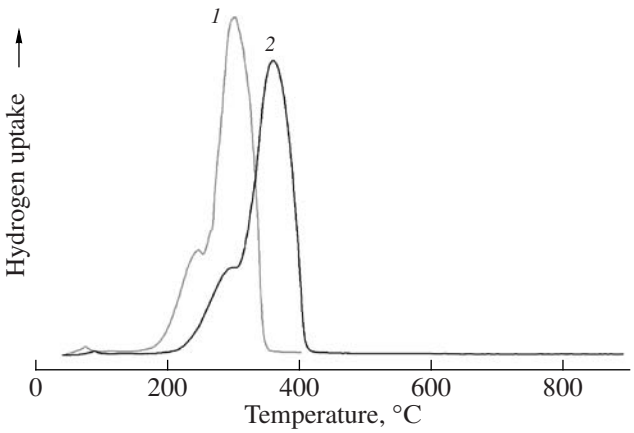

Fig. 3. TPR curves for Co_3O_4(1) at heating rates of (*1*) 2 and (*2*) 10 K/min.

temperatures (determined based on the appearance of reflections from the hcp Co phase) of single-phase samples were 190, 210, and 190°C for Co_3O_4(1), Co_3O_4(2), and Co_3O_4(3), respectively; that is, the minimum reduction temperatures of the model samples were close to each other. For the supported sample Co_3O_4/γ-Al_2O_3(5), the temperature of the onset of reduction in 100% H_2 (the appearance of reflections from the CoO phase) was 180°C. Reflections from fcc Co appeared only as the temperature was further increased to 260°C.

Nevertheless, cobalt oxide was incompletely reduced to cobalt metal even at 350°C (usual reduction temperature in a commercial reactor) (Fig. 2). In addition to cobalt metal, the XRD patterns exhibited reflections from the CoO phase. In the reduction of the supported cobalt oxide Co_3O_4/γ-Al_2O_3(5), the average CSR sizes for CoO were 80 and 40 Å at $T = 260$ and 350°C, respectively; the average CSR size for fcc Co over the temperature range of 300–400°C was about 70 Å. Thus, we found using XRD analysis that the average CSR sizes for supported CoO decreased in the course of reduction.

This is consistent with published data [7, 14, 15], according to which relatively coarse CoO particles weakly bound to the support are easily reduced to Co metal, whereas small cobalt oxide crystallites strongly bound to the support are difficult to reduce; that is, they are reduced at sufficiently high temperatures.

Temperature-programmed reduction. To examine the reduction process, we studied Co_3O_4(1) and Co_3O_4/γ-Al_2O_3(5) using TPR (Figs. 3, 4).

Figure 3 shows the TPR curve for the sample Co_3O_4(1), which exhibits two peaks. The temperatures of the onset of reduction were 210 and 190°C at heating rates of 10 and 2 K/min, respectively. The presence of two peaks with an area ratio of 1 : 3, which corresponds to the reaction stoichiometry, suggests that the reduction process occurs in two steps under these conditions:

$$Co_3O_4 + H_2 \longrightarrow 3CoO + H_2O;$$

$$CoO + H_2 \longrightarrow Co + H_2O.$$

The TPR curve for the supported sample (Fig. 4) exhibits three clearly pronounced peaks. The ratio of the first peak area to the sum of the second and third peak areas is 1 : 3. Thus, the first peak can be ascribed to the reduction of Co_3O_4 to CoO, and the second and third peaks can be attributed to the formation of cobalt metal from CoO. From these data, it follows that two states of CoO occurred in this sample; one of them is more readily reduced to cobalt metal and the other is reduced at higher temperatures (as will be demonstrated below, because of the interaction with the support).

In situ XRD study in a flow of 6% H_2 + 94% He. At first glance, a contradiction appears between the TPR data obtained in an atmosphere of 10% H_2 + 90% Ar and the results of diffraction experiments performed

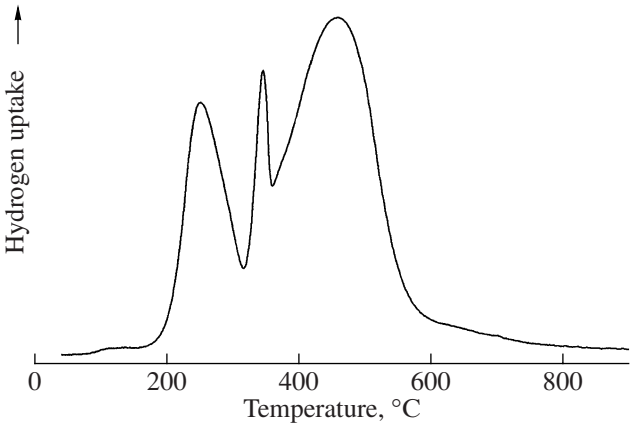

Fig. 4. TPR curve for Co_3O_4/γ-Al_2O_3(5).

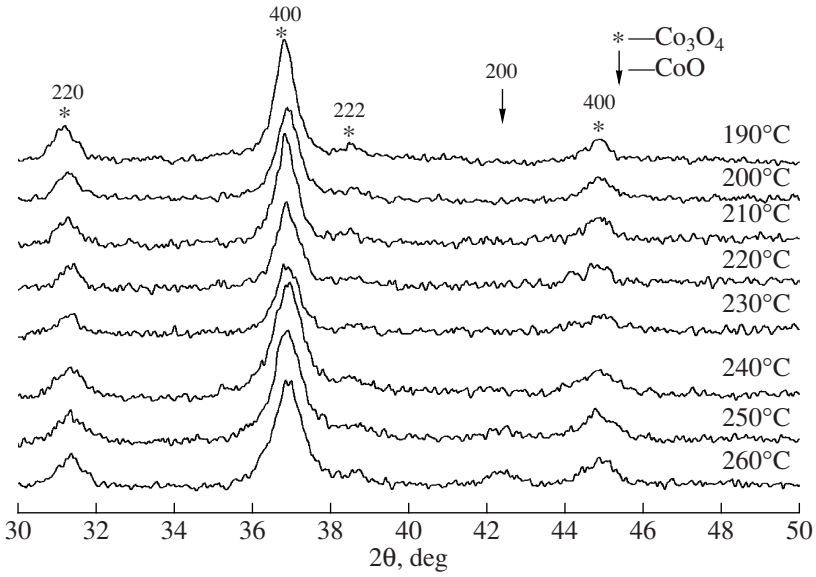

Fig. 5. XRD patterns of Co_3O_4(1) upon reduction with a mixture of 6% H_2 + 94% He at 190–260°C.

in an atmosphere of undiluted hydrogen. Therefore, we performed an additional in situ XRD experiment in an atmosphere of hydrogen diluted with helium (6% H_2 + 94% He). Figure 5 shows the diffraction patterns for the sample Co_3O_4(1) at 190–280°C in a flow of 6% hydrogen in helium. It can be seen that the appearance of an additional peak ($2\theta = 42.36°$) was observed $T = 250°C$; this peak corresponds to the reflection (200) of the CoO phase. The final product of reduction is cobalt metal with the hcp structure.

The experimental results indicate that differences between the results obtained by different methods in the reduction of model samples are related to the concentration of hydrogen.

According to XRD data, the reduction of Co_3O_4(1) in pure hydrogen to cobalt metal occurred in a single step without the formation of the crystalline phase of CoO, whereas a two-step process was clearly observed at a hydrogen content of 6–10%. It is likely that the reduction process competed with the formation of the crystalline phase of CoO.

Differential dissolution. The composition of the difficult-to-reduce portion of cobalt oxide in the supported catalyst can be determined using differential dissolution. Differential dissolution data (Table 3) for the initial (unreduced) sample of Co_3O_4/γ-Al_2O_3 allowed us to distinguish between the two main states of cobalt: the phase of a mixed Co–Al compound and the phase of a cobalt compound dissolvable under much more severe conditions. The latter phase was associated with the XRD-observable phase of Co_3O_4 (Table 3). The stoichiometry of the mixed phase corresponds to the ratio Co/Al = 0.05 : 1. We quantitatively estimated that about 36% cobalt and 93% aluminum (on a total basis) occurred in this phase in the sample. The results of the differential dissolution of the reduced sample were much different from the corresponding data for the initial sample. A peak due to the difficultly soluble phase of Co_3O_4 (dissolution interval from 75 to 85 min) was absent; however, a readily soluble phase containing 86% supported cobalt appeared. Evidently, this cobalt-containing phase is the CoO oxide. First, according to the XRD data, this oxide was partially retained in the reduced sample; second, it was formed by the reoxidation of cobalt metal particles in air. A Co–Al compound containing 10% cobalt and 2% aluminum (on a total basis) with the ratio Co/Al = 2 : 1 was also present. It is likely that this phase was not detected by XRD analysis because of very small particle sizes. However, as judged from the ratio between the cations, this can be a spinel-type phase of Co_2AlO_4. A phase containing 90% aluminum and 4% cobalt with the Co/Al ratio varied from 0.005 : 1 to 0.02 : 1 was also present in the reduced sample. Comparing the XRD and differential dissolution data, we can hypothesize that the last phase was a solid solution of cobalt in γ-Al_2O_3.

Electron microscopy. The electron microscopic image of Co_3O_4/γ-Al_2O_3 (5) (Fig. 6) exhibits cobalt oxide particles (contrast spots) together with γ-Al_2O_3. The sizes of individual Co_3O_4 particles corresponded to the X-ray CSR values of 10–15 nm. It can be seen that Co_3O_4 crystallites (with a regular structure) and γ-Al_2O_3 blocks join each other to form developed interfaces. It is likely that cobalt ions diffused into the structure of γ-Al_2O_3 at these interfaces to form a mixed Co–Al oxide at the boundary. This mixed oxide, which was detected by differential dissolution, is difficult to reduce later on.

Note that the reduction of the Co_3O_4 portion that was weakly bound to the support occurred differently

Table 3. Phase compositions of the initial and reduced $Co_3O_4/\gamma\text{-}Al_2O_3(5)$ according to XRD and differential dissolution data

Sample $Co_3O_4/\gamma\text{-}Al_2O_3(5)$	Phase composition according to XRD data	Phase composition according to differential dissolution data			
		dissolution interval, min	cationic composition of the dissolved phase	element concentration*, %	
				Co	Al
Initial	Co_3O_4,	0–55	Al	–	7
	$\gamma\text{-}Al_2O_3$	55–70	$Co_{0.05}Al_1$	39	93
		70–85	Co	61	
Reduced in a flow of hydrogen for 4 h	CoO,	5–25	Co	86	–
	Co(fcc),	5–25	Al	–	8
	$\gamma\text{-}Al_2O_3$	25–35	Co_2Al_1	10	2
		50–75	$Co_xAl_1^{**}$	4	90

Notes: * With respect to the total element concentration in the sample.
$x = 0.005–0.02$ (variable-composition phase).

from the reduction on the single-phase samples. Indeed, the phase of cobalt metal was not detected in the supported samples immediately after the onset of reduction ($T = 190°C$), as in the case of the single-phase samples. Evidently, the effect of the support was not restricted by the formation of an interaction phase. The occurrence of this phase cannot explain the fact that the reduction of model and supported samples under identical conditions (unreduced hydrogen) occurred through different steps and led to different products. Thus, the reduction of supported samples occurs in two steps: at the first step, Co_3O_4 is converted into CoO; at the second step, CoO is reduced to Co metal (fcc). In the model samples of Co_3O_4, the complete reduction to Co metal (hcp) occurs in a single step without the formation of the crystalline phase of CoO.

It is of interest that, in the reduction of supported cobalt oxide, the formation of a cobalt metal phase (fcc) occurs at 260°C, whereas Co (hcp) is considered stable at this temperature. The conversion of one cobalt modification into another occurs at ~400°C. To 400°C, α-cobalt with an hcp structure is stable, and β-cobalt with an fcc structure is stable above 400°C. The conversion of α-cobalt into β-cobalt on heating occurs slowly, and it is accompanied by heat absorption [16].

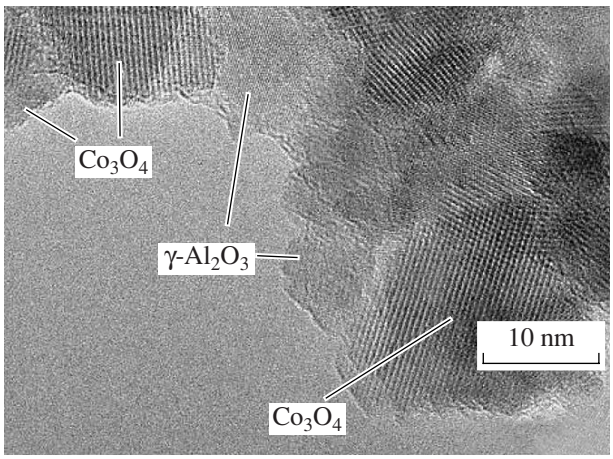

Fig. 6. Electron micrograph of the sample $Co_3O_4/\gamma\text{-}Al_2O_3(5)$.

It is likely that the formation of a high-temperature cobalt modification is related to local overheating. The reduction reaction occurs with the release of heat; therefore, a temperature sufficient for the formation of a high-temperature cobalt metal modification can be reached in the bulk of the sample.

CONCLUSIONS

Our studies of cobalt oxide samples performed with the use of a set of techniques allowed us to consider in detail the reduction of these samples with hydrogen. We characterized the structures of Co_3O_4 in model and supported catalysts. The structure is defect (Co/O = 0.57–0.64) and contains vacancies in octahedral and tetrahedral positions of the spinel structure. It is likely that the nonstoichiometry of the samples is due to the presence of residual anion groups. The reduction of both samples under conditions of our experiments began at ~190°C. However, the reduction of model and supported samples occurred through different steps and led to different products. In the supported samples, the reduction process occurred in two steps: at the first step, Co_3O_4 was converted into CoO; at the second step, CoO was reduced to Co metal (fcc) with the remaining unreduced cobalt oxide phase. The reduction to metal was hindered because of the presence of the interaction phase of cobalt oxide with the $\gamma\text{-}Al_2O_3$ support.

The reduction of the single-phase samples of Co_3O_4 in undiluted hydrogen to Co metal (hcp) occurred without the formation of the crystalline CoO phase. At the same time, the reduction occurred in two steps at lower

partial pressures of hydrogen (6–10% H_2 + an inert gas).

ACKNOWLEDGMENTS

We are grateful to Cand. Sci. (Chem.) V.A. Rogov for performing TPR experiments and to Dr. Sci. (Chem.) L.A. Isupova for providing us with samples.

REFERENCES

1. Storch, H.H., Golumbic, N., and Anderson, R.B., *The Fischer–Tropsch and Related Syntheses*, New York: Wiley, 1951.
2. Arnoldy, P. and Moulijn, J.A., *J. Catal.*, 1985, vol. 93, p. 38.
3. Vob, M., Borgmann, D., and Wedler, G., *J. Catal.*, 2002, vol. 212, p. 10.
4. Bessell, S., *Appl. Catal., A*, 1993, vol. 96, p. 253.
5. Jacobs, G., Chaney, J.A., Patterson, P.M., Das, T.K., and Davis H.B., *Appl. Catal., A*, 2004, vol. 264, p. 203.
6. Rosynek, M.P. and Polansky, C.A., *Apl. Catal., A*, 1991, vol. 73, p. 97.
7. Jacobs, G., Das, T.K., Zhang, Y., Li, J., Racoillet, G., and Davis, B.H., *Apl. Catal., A*, 2002, vol. 223, p. 263.
8. Lin, H.-Y. and Chen, Y.-W., *Mater. Chem. Phys.*, 2004, vol. 58, p. 171.
9. Leite, L., Stonkus, V., Edolfa, K., Ilieva, L., et al., *J. Mol. Catal.*, 2004, vol. 215, p. 95.
10. Zhang, Y., Wei, D., Hammache, S., and Goodwin, J.G., *J. Catal.*, 1999, vol. 188, p. 281.
11. Malakhov, V.V., *Zh. Anal. Khim.*, 2002, vol. 57, no. 10, p. 1029 [*J. Anal. Chem.* (Engl. Transl.), vol. 57, no. 10, p. 869].
12. Malakhov, V.V., Vlasov, A.A., and Dovlitova, L.S., *Zh. Anal. Khim.*, 2004, vol. 59, no. 11, p. 1126 [*J. Anal. Chem.* (Engl. Transl.), vol. 59, no. 11, p. 1016].
13. Vishnevskii, A.L., Molchanov, V.V., Kriger, T.A., and Plyasova, L.M., *Int. Conf. on Powder Diffraction and Crystal Chemistry*, St. Petersburg, 1994, p. 206.
14. Bessell, S., *Appl. Catal., A*, 1993, vol. 96, no. 2, p. 253.
15. Sexton, A., Hughes, A.E., and Turney, T.W., *J. Catal.*, 1986, vol. 97, no. 2, p. 390.
16. Barrett, C.S. and Massalski, T.B., *Structure of Metals*, Oxford: Pergamon, 1980.